Slow Crack Growth During Radiative Cooling of LHG8 and BK7 Plates

Introduction

Because of their low resistance to fracture and low thermal conductivity, many ceramics and glasses are susceptible to thermal shock. A common thermal shock configuration consists of a component at an initially uniform high temperature suddenly exposed to a cooling medium at a lower temperature. The more-rapid temperature decrease at the surface induces a tensile stress, while the component's interior is in a state of compression. Kingery[1,2] has discussed in detail the effects of material and cooling medium properties on thermal shock. The relevant figures of merit governing thermal shock have been reviewed by Hasselman[3] and Wang and Singh.[4]

Depending on the thermal conductivity of the component, its dimensions, and the heat transfer coefficient induced by the cooling medium, there may exist a state of "severe" thermal shock (where the tensile thermal stresses at the component surface depend only on the material's thermomechanical properties) or "mild" thermal shock (where the surface tensile stresses depend on the material's thermomechanical properties and the Biot number, involving the cooling heat transfer coefficient, specimen size, and component thermal conductivity). The heat transfer coefficient itself depends on the flow between the component and the cooling medium (forced or natural), the dimensions of the component, and the cooling medium's thermophysical properties (viscosity, density, and thermal diffusivity). The conditions for severe or mild thermal shock along with an extensive discussion of the contributions of the thermomechanical properties can be found in Refs. 5–7.

Since the Biot number is an important factor in determining the severity of thermal shock, ceramics and glasses behave differently under thermal shock conditions. Ceramics have higher thermal conductivity and, therefore, lower Biot numbers, leading to conditions prone to mild thermal shock. Glasses, on the other hand, have a low thermal conductivity and are thus liable to severe thermal shock. A large amount of work exists in the literature on thermal shock of ceramics[3–9] but less on thermal shock of glasses.[10]

This article discusses the radiative cooling of two optical glasses: the borosilicate crown BK7 and the phosphate LHG8. Under radiative cooling conditions, the usual thermal shock analysis does not apply because the surrounding temperature continuously changes with time as does the heat transfer coefficient (and thus the Biot number). We determine the relevant thermal and stress fields numerically using finite elements and then use these results to study crack growth at the heaviest stressed locations. We discuss fracture in terms of strength, fracture toughness, and slow crack growth under transient temperature and stress fields.

Material Properties

The two materials investigated here are the borosilicate crown glass BK7, a commonly used optical glass, and the phosphate glass LHG8 often used in laser applications. The glass properties are listed in Table 119.II.

We observe that LHG8 is about twice as brittle in terms of fracture toughness K_c as BK7, while it is also twice as soft. In Table 119.II, we have also calculated the fracture strength for these glasses, assuming different sizes of initial flaw size into the surface. Table 119.II gives a range for the fracture toughness of LHG8. The higher value $\left(0.51\ \text{MPa}\sqrt{\text{m}}\right)$ is cited in Campbell *et al.*,[11] while the lower value $\left(0.43\ \text{MPa}\sqrt{\text{m}}\right)$ is cited in DeGroote *et al.*[12] Notice, however, that a typical uncertainty in K_c is ±10%. In this sense, these measurements agree.

Suratwala *et al.*[13] have measured the slow crack growth in LHG8 using the double-cleavage-drilled-compression method. They showed that the rate of crack growth v depends on the amount of OH concentration in the glass. They reported data in the temperature range of 25°C to 300°C and water vapor pressure in the range of 2 to 92 mmHg. These data can be fitted by

$$v = \frac{v_I v_{II}}{v_I + v_{II}} \tag{1}$$

Table 119.II: Material properties of the two glasses studied.

Property and Units	BK7	LHG8
Density ρ, kg/m^3	2510	2830
Heat capacity cp, J/kg.K	858	750
Thermal conductivity k, W/m.K	1.114	0.58
Thermal diffusivity D, m^2/s	5.2×10^{-7}	2.7×10^{-7}
Young's modulus E, GPa	82	50
Poisson ratio ν	0.21	0.26
CTE α, K^{-1}	8.3×10^{-6}	12.7×10^{-6}
Fracture toughness K_c, MPa$\sqrt{\text{m}}$	0.82	0.43 to 0.51
Fracture strength, MPa (assumes scratch a is 50 μm deep)	59	31 to 36
Fracture strength, MPa (assumes scratch a is 500 μm deep)	19	10 to 12
Fracture strength, MPa (assumes scratch a is 1000 μm deep)	13	7 to 8
Hardness, GPa	6.8±0.3	3.4

with

$$v_I = v_0 \left(\frac{p_{H_2O}}{p_0} \right)^m \exp\left(\frac{K_{app} b - Q_I}{RT} \right),$$
$$v_{II} = C \frac{p_{H_2O}}{p_0} \exp\left(\frac{-Q_{II}}{RT} \right), \tag{2}$$

where p_0 is the atmospheric pressure 760 mmHg. The parameters are listed in Table 119.III. The subscripts I and II correspond to region I (stress controlled) and region II (diffusion controlled) crack growth.[13,14] The harmonic mean in Eq. (1) essentially selects the lower of v_I, v_{II}. Notice that the applied stress intensity factor K_{app} affects the crack growth rate v_I (but not v_{II}).

For the case of a quarter circular crack at the edge of a plate under tension, the applied stress intensity factor is

$$K_{app} = \Omega \, \sigma_{app} \sqrt{\pi a}, \tag{3}$$

where Ω is a geometrical factor (~0.80), σ_{app} is the applied tension, and a is the crack depth (see Lambropoulos *et al.*[15] for the geometrical factor Ω describing a quarter circular crack along an edge).

For the case of BK7, we used the data of Wiederhorn and Roberts,[14] who measured slow crack growth in BK7 and other glasses with a double cantilever beam technique. They reported data for BK7 at temperatures of 23°C, 104°C, 154°C, and 226°C under vacuum (10^{-5} Torr), as well as for BK7 in air and RT under 100% RH.

Table 119.III: Data for slow crack growth in LHG8 from Suratwala *et al.*[13]

Parameter	Units	LHG8-L (128-ppmw OH)	LHG8-H (773-ppmw OH)
v_0	10^6 m/s	7.3	7.3
m	dimensionless	1.20	1.20
Q_I	kJ/mol	253	239
b	m$^{5/2}$/mol	0.48	0.48
C	m/s	180	180
Q_{II}	kJ/mol	26	26

For numerical computation, we have fitted the data at the crack growth rates of 10^{-5} m/s, 10^{-6} m/s, and 10^{-7} m/s for these four temperatures. We fitted these data to the form

$$v_I = v_0 \exp\left(\frac{K_{app} b - Q}{RT}\right) \tag{4}$$

by a numerical procedure that minimized the error, defined as

$$\%\text{error}(v_0, b, Q) = 100 \times \frac{\sum_1^{12} \left[\ln v(v_0, b, Q) - \ln v_i\right]^2}{\sum_1^{12} (\ln v_i)^2}. \tag{5}$$

The best fit gave a minimum error of 0.62% and corresponded to the parameters

$$\begin{aligned} \ln v_0 &= 10.10, \\ b &= 0.21 \text{ m}^{5/2}/\text{mol}, \\ Q &= 227.5 \text{ kJ/mol}, \end{aligned} \tag{6}$$

describing the slow crack growth of BK7 at "vacuum" conditions. These data will be used to predict crack growth in BK7 under vacuum conditions.

Finite Element Analysis: Temperature and Stress

Both materials modeled are in the form of rectangular plates with an areal extent of 800 × 400 mm^2. The BK7 plates are 80 mm thick; the LHG8 plates are 40 mm thick. These dimensions will be consistent throughout the remainder of our work. The BK7 and LHG8 thicknesses are different because thermal stress is known to scale with thickness, while LHG8 is less strong than BK7. In a sense, therefore, the stronger BK7 plates are more severely stressed than the thinner LHG8.

The plate was initially placed in an oven at a uniform high temperature. The oven temperature slowly diminished with time, so that all six sides of the plate underwent radiative cooling into an ambient whose temperature changed with time. In both cases of LHG8 and BK7, it was assumed that the initial temperature was uniform and equal to a high value of 200°C. The surroundings' (ambient) temperature decayed exponentially with a time constant τ that may vary from minutes to hours to days. The eventual temperature was room temperature, again taken as uniform (see Fig. 119.28).

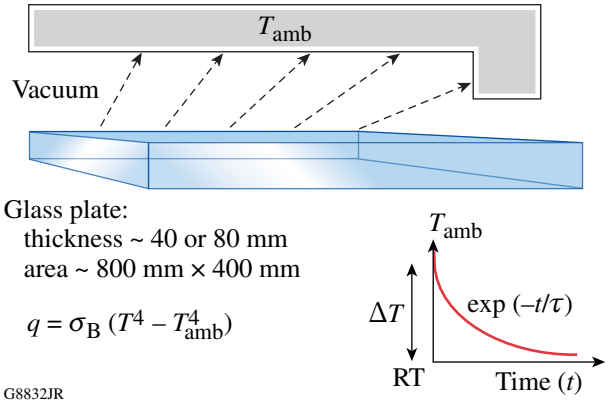

Figure 119.28
The geometry of a thin plate cooled by radiation. The ambient temperature decayed exponentially from the initial temperature of 200°C to the final temperature (RT) with a time constant τ.

The coordinate system was centered at the plate's center, with –400 mm < y < 400 mm, –200 mm < x < 200 mm, and the coordinate z varying –20 mm < z < 20 mm for LHG8 or –40 mm < z < 40 mm for BK7.

The boundary condition on all six edges of the glass plate was taken as radiating into a medium of ambient temperature $T_{amb}(t)$, i.e.,

$$q\left[\text{W}/\text{m}^2\right] = \sigma_B\left(T^4 - T_{amb}^4\right), \tag{7}$$

where σ_B is the Boltzmann constant 5.67 × 10^{-8} W/(m^2.K^4), T is the absolute temperature at the glass surface, and T_{amb} is the (time-dependent) temperature of the surroundings (ambient), taken to vary as

$$T_{amb}(t) = 293 + 180 \exp\left(-t/\tau\right), \tag{8}$$

where the time constant τ models the rate at which the surroundings temperature decays with time. The ambient temperature drops from 200°C to 86°C in time τ and to 29°C in time 3τ. The initial condition is

$$T(x, y, z, t = 0) = 473 \text{ K}. \tag{9}$$

The temperature $T(x,y,z,t)$ is governed by the time-dependent, 3-D heat conduction equation. A typical temperature evolution is shown in Fig. 119.29.

Once the temperature was determined, the stresses were calculated by using COMSOL® (version 3.4).[16] We note some

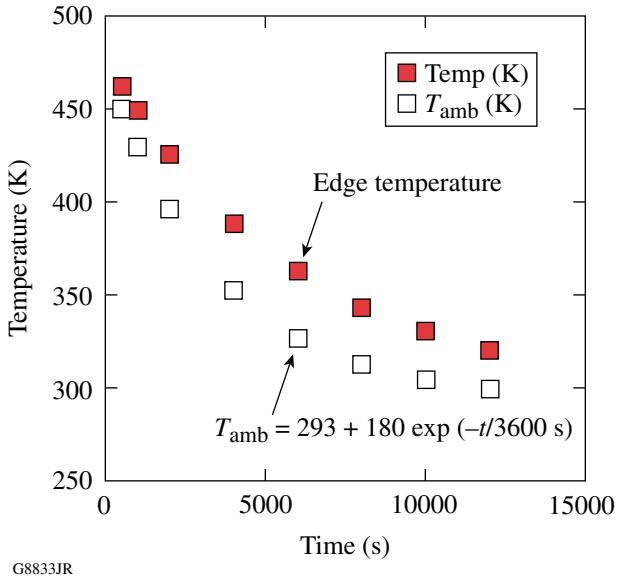

Figure 119.29
Temperature evolution along the edge center of the long edge in a 40-mm-thick LHG8 plate. The temperature relaxation constant τ = 1 h. The ambient temperature is also shown.

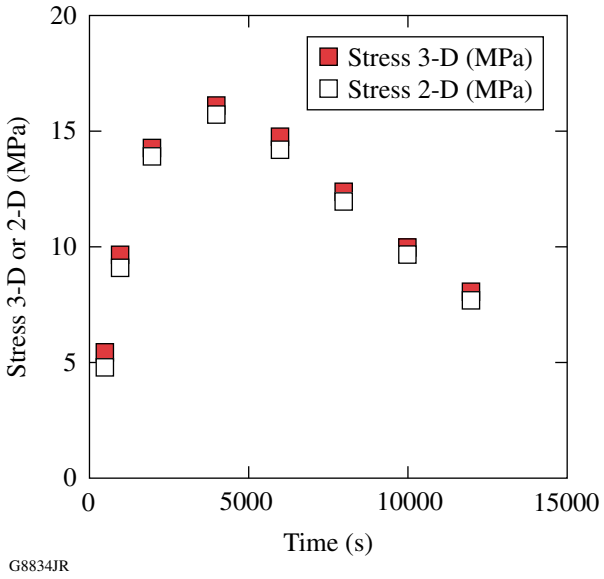

Figure 119.30
Thermal stress evolution along the edge center of the long edge in a 40-mm-thick LHG8 plate. The temperature relaxation constant τ = 1 h. For short times, the temperature was high and uniform, so the thermal stress was low. These results show the thermal stress calculated via 3-D or 2-D (plane-strain) approaches. Both approaches give similar stress levels.

features of the resulting stress distribution: At early times, the temperature was high but mostly uniform; therefore the thermal stress was very small. At long times, the temperature was low and again mostly uniform; therefore the thermal stress was also low. As a result, the thermal stress became largest at some intermediate time. An example of stress evolution along the center of the long edge is shown in Fig. 119.30.

We also observed that the Biot number was neither small nor very large. To extract an applicable heat transfer coefficient h_{eff}, we linearized the surface-cooling constitutive law to read

$$q\left[\text{W}/\text{m}^2\right] = 4\sigma_B T_{\text{amb}}^3 \left(T - T_{\text{amb}}\right) = h_{\text{eff}}\left(T - T_{\text{amb}}\right). \quad (10)$$

Evaluating h_{eff} at T_{amb} = 473 K or at 300 K, we found that h_{eff} was in the range of 24 to 26 W/m^2.K, so that the Biot number

$$\text{Bi} = h_{\text{eff}} L/k \quad (11)$$

(with 2L as the plate thickness) was in the range of 0.2 to 0.8 for LHG8 and 0.2 to 0.9 for BK7. We concluded that the temperature gradients in the plate cannot be neglected and indeed must explicitly be accounted for.

Notice that if h_{eff} were very large (i.e., if Bi $\gg$ 1, corresponding to very rapid quenching by ΔT), the surface thermal stress would be

$$\sigma_{\max} = \frac{\alpha E \Delta T}{1 - \upsilon} \quad (12)$$

with ΔT representing the temperature drop (here 180°C), α the coefficient of thermal expansion, and E the Young's modulus. This estimate would give a stress of about 150 MPa for either BK7 or LHG8, i.e., a stress significantly higher than the strength of the glass (see Table 119.II). The fact, however, that the applicable Biot number Bi is of the order of 1 means that such estimates of stress as in Eq. (12) are not applicable and stresses must be explicitly computed.

Figure 119.31 shows the stress distribution in LHG8 cooled at the rate τ = 4 h. The long and intermediate edges of the plate were the most highly stressed. Figure 119.32 compares directly the evolution of temperature and stress at the center of the long edge for a plate of LHG8 and a plate of BK7. Strong size effects (i.e., increasing stresses with increasing plate thickness) and rate effects (i.e., stresses increasing with more-rapid cooling), from extensive stress calculations by finite element methods, are shown for LHG8 in Fig. 119.33.

We will next determine how a surface flaw in the most heavily stressed area (the center of the long edges) will grow as the temperature and stress evolve at that point. To examine

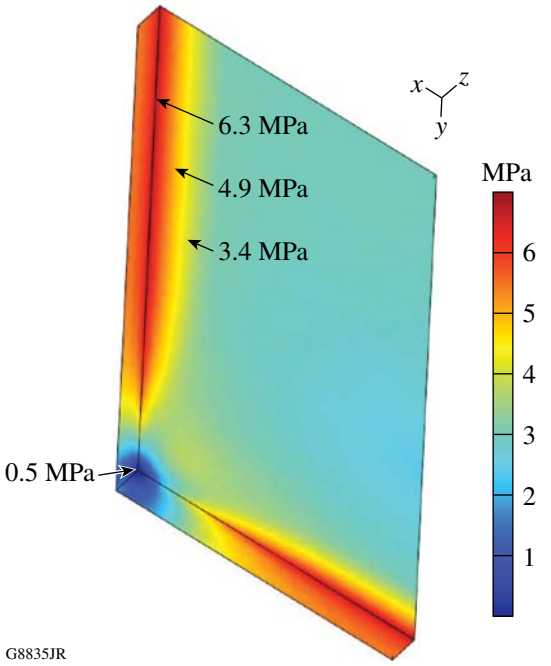

Figure 119.31
Thermal stress distribution at time $t = 8000$ s (about 2.2 h) in a 40-mm-thick LHG8 plate. Only 1/8 of the plate is shown. The plot shows the maximum principal stress, at a time when the thermal stress at the edge was close to maximum. The temperature relaxation constant $\tau = 4$ h. The long edges at $x = \pm 200$ mm, $y,z = \pm 20$ mm and intermediate edges at $x,y = \pm 400$ mm, $z = \pm 20$ mm were in a state of tension of magnitude 6.9 MPa. The plate's long edges and intermediate edges were similarly stressed and the stresses at these locations were the highest.

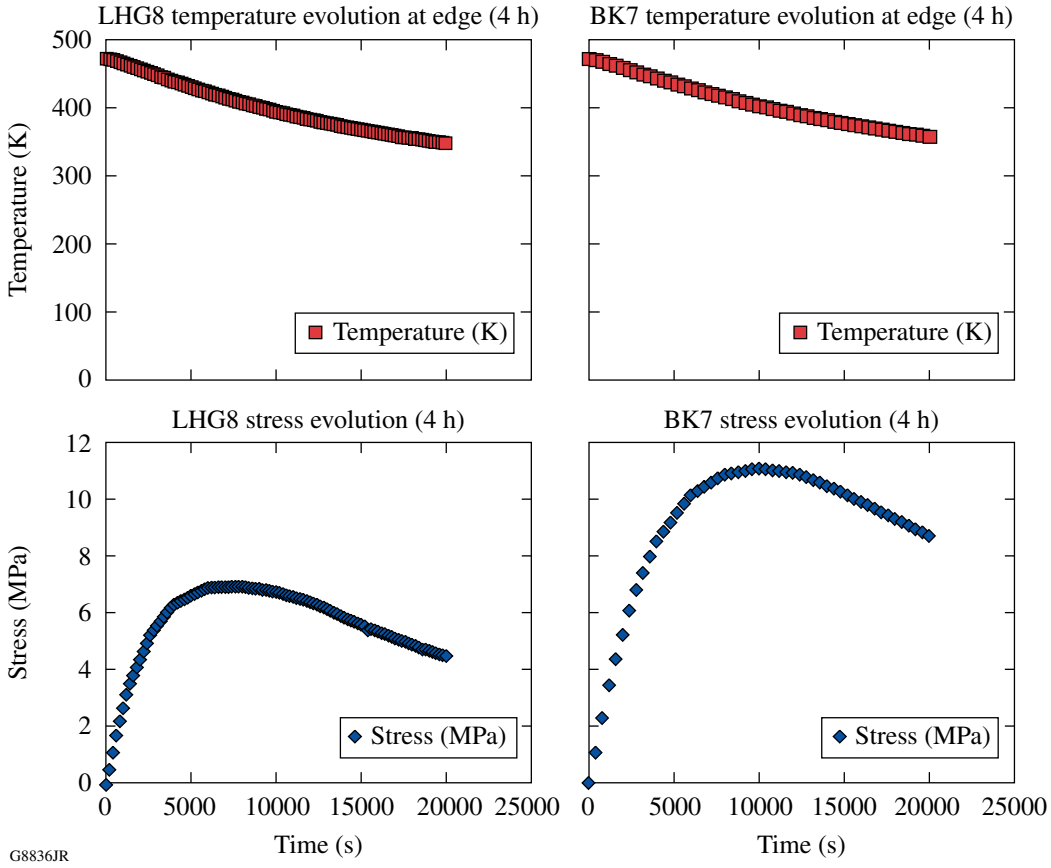

Figure 119.32
The evolution of temperature at the center of the long edge and the stress at the same point for plates of LHG8 (40 mm thick) and BK7 (80 mm thick). In both cases, the time constant for the oven temperature decay was $\tau = 4$ h.

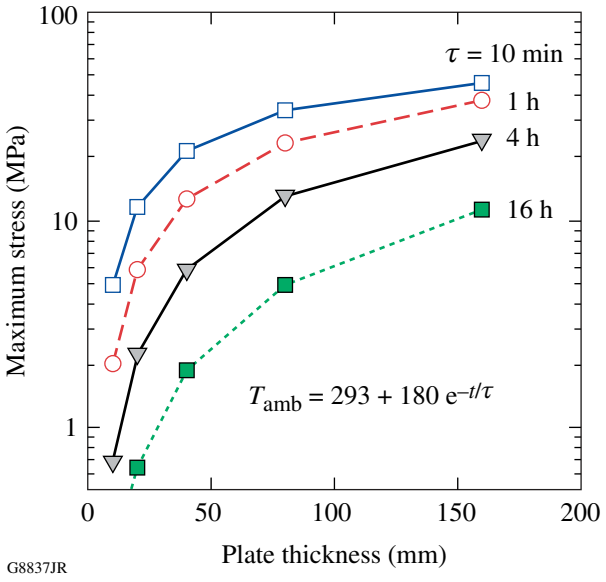

Figure 119.33
The maximum thermal stress (occurring at the center of the long plate edges) depends on the plate thickness and the rate at which the ambient temperature decays. These results are for the case of LHG8 glass plates. Thicker plates lead to larger stresses, as do more-rapid temperature cooling rates.

crack growth we need two auxiliary results: first, the depth of the initial flaw in the glass long edge (a figure to be estimated from the abrasive size used to finish that edge); second, a way of describing crack growth, from that initial crack depth value, as temperature and stress evolve with time.

It is important here to keep distinct the terminology of the various types of cracks resulting from finishing the plate surfaces. By subsurface damage (SSD) we mean the average flaw depth, a quantity that can be estimated from the abrasive used to finish that edge or from the peak-to-valley roughness at that point. This is different from the deepest flaw size $\langle c \rangle_{\max}$, which will control the strength at that point.

We have shown in previous work on glasses and crystals[17] that the subsurface damage can be estimated from the abrasive used to finish a surface by

$$\text{SSD} \sim 2 \times (\text{abrasive size}). \tag{13}$$

On the other hand, Suratwala *et al.*[18] have shown that the maximum flaw depth in fused silica is about 8× the average flaw depth:

$$\langle c \rangle_{\max} \sim 8 \langle c \rangle_{\text{av}}. \tag{14}$$

By identifying the average crack depth $\langle c \rangle_{\text{av}}$ with the subsurface damage SSD, we arrive at

$$\langle c \rangle_{\max} \sim 16\times (\text{abrasive size}). \tag{15}$$

For example, when finishing with 15-μm abrasives, one would expect a 240-μm flaw depth into the glass surface.

Notice here that the relation between average and deepest flaw size in Eq. (14) was measured[18] for the case of fused silica and its applicability to LHG8 and BK7 is not known. On the other hand, these estimates are for finishing flat surfaces. Given the fact that the area most heavily stressed is the edge of the plate (i.e., the intersection of two flat surfaces), it is again not entirely clear how to extend Eqs. (13)–(15) to our case. In any case, we must keep these caveats in mind while estimating the deepest flaw at the edge by Eq. (15).

Cracking in LHG8 Versus BK7

For fracture in radiatively cooled BK7 and LHG8 plates, we adopted several different approaches. In the strength approach, fracture was taken to occur when the applied stress σ_{app} reached the fracture strength of the glass σ_{F}. Therefore, for safe operation, we required

$$\sigma_{\text{app}} < \sigma_{\text{F}} \Rightarrow \text{safe}. \tag{16}$$

For a typical glass, the figure of merit for strength is about 50 MPa. As shown in Table 119.II, the strength of LHG8 is 10 MPa, while the strength of BK7 is 20 MPa. The applied stresses are shown in Fig. 119.32. For LHG8 the maximum stress is 7 MPa, while for BK7 it is 11 MPa. The conclusion is that, based on the strength approach, both LHG8 and BK7 are safe under these cooling conditions.

The main drawback of this approach is that the strength of a glass surface is not a well-described quantity. This drawback is addressed by using the fracture toughness approach.

In the fracture toughness approach, cracking will occur when the applied stress intensity factor K_{app} reaches the material's fracture toughness for a given flaw size. The applied stress intensity is given by Eq. (3). Therefore, for safe operation, we require

$$K_{\text{app}} = \Omega\, \sigma_{\text{app}} \sqrt{(\pi a)} < K_{\text{c}}, \quad \text{or } a < \frac{1}{\pi}\left(\frac{K_{\text{c}}}{\Omega\, \sigma_{\text{app}}}\right)^2. \tag{17}$$

For a quarter circular crack along an edge, $\Omega = 0.80$ (Ref. 15). Using $K_c = 0.43$ to 0.51 MPa$\sqrt{\text{m}}$ for LHG8 and $\sigma_{app} = 7$ MPa (from Fig. 119.32), we conclude that any flaw size more shallow than 1.9 to 2.7 mm is safe. Repeating for BK7 with $\sigma_{app} = 11$ MPa from Fig. 119.32, we find that any flaw size $a < 2.8$ mm is safe.

The drawback of the fracture toughness approach is that it assumes that the fracture toughness is a property that is independent of temperature.

For the slow crack growth approach, crack growth evolves according to

$$\frac{da}{dt} = F\left\{K_{app}\left[a(t)\right], T(t)\right\}, \tag{18}$$

$$K_{app}(t) = \Omega\, \sigma_{app}(t)\sqrt{\pi a(t)}, \tag{19}$$

where the function F is given by Eq. (1) or (4), and the stress $\sigma_{app}(t)$ and temperature $T(t)$ are shown in Fig. 119.32.

The data for LHG8 were modeled with the following parameters (see **Material Properties**, p. 145):

$$\begin{aligned} v_0 &= 7.3 \times 10^6 \text{ m/s}, \\ b &= 0.48 \text{ m}^{5/2}/\text{mol}, \\ Q_I &= 239 \text{ kJ/mol} \end{aligned} \tag{20}$$

(corresponding to LHG8 with higher OH concentration and, therefore, greater propensity for cracking). It is also important here to note that although the fit in Eq. (2) is for any pressure and the pressure in the oven is "vacuum," we have used the slowest experimental data reported,[14] i.e., we have taken $p_{H_2O} = 2$ mmHg.

For the case of BK7, we repeat the procedure for F given by Eq. (4) with

$$\begin{aligned} v_0 &= 2.4 \times 10^4 \text{ m/s}, \\ b &= 0.21 \text{ m}^{5/2}/\text{mol}, \\ Q_I &= 227.5 \text{ kJ/mol}. \end{aligned} \tag{21}$$

In both cases, the crack growth rate depends on the depth of the initial flaw size. If the initial crack depth is too deep, the crack will grow catastrophically at some time, leading to a complete fracture of the plate. We have numerically determined an initial flaw size that is just below this critical condition.

Figure 119.34 shows the critical growth condition for LHG8. The initial crack size was about 970 μm. Any crack size deeper than this will lead to catastrophic failure of the plate. It is seen that crack growth has three regions: For early times, there is little growth because the thermal stress is low. For very long times, crack growth is also low because the temperature is low. For intermediate times, however, crack growth is appreciable because both stress and temperature are sufficiently high. For the case of LHG8, the final crack size will be about 1200 μm, but the plate will not fail catastrophically.

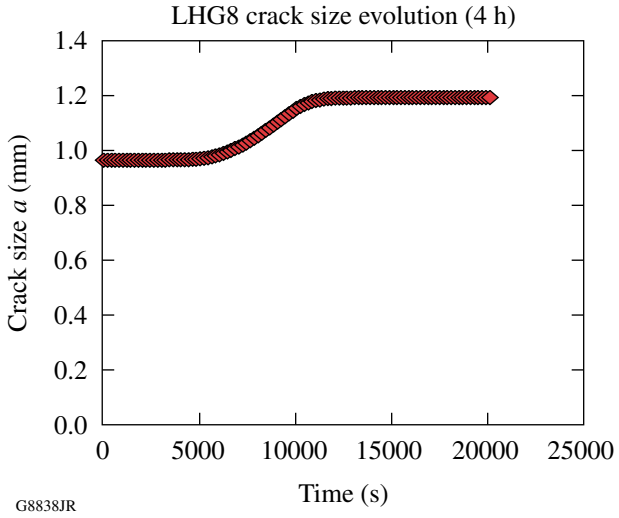

Figure 119.34
Crack growth in the center of the long edge of a 40-mm-thick LHG8 plate. The initial flaw size was 970 μm. Any flaw size deeper than this will lead to catastrophic failure.

A similar analysis for the BK7 plate leads to the conclusion that for BK7 the critical initial flaw depth was 1650 μm.

The predicted crack growth rate for LHG8 is shown in Fig. 119.35. Notice that there is an initial incubation period (temperature was high but stresses were low) and a final period at which crack growth stopped (the temperature was too low). The crack growth rate was largest, about 50 to 60 nm/s, for intermediate times where both temperature and stresses were significant; indeed, this was slow crack growth.

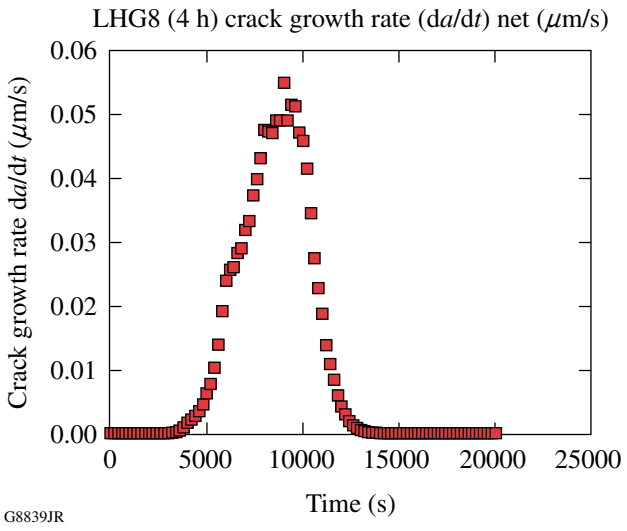

Figure 119.35
Predicted crack growth rate at the midpoint of the long edge of a 40-mm-thick LHG8 plate. The initial flaw size was 970 μm. Any flaw size deeper than this will lead to catastrophic failure.

We observe that although BK7, being twice as thick as LHG8, has higher thermal stresses, it has slower crack growth behavior and can tolerate cracks up to 1650 μm along the center of its long edge. LHG8 can tolerate cracks only up to 970 μm.

The slow crack growth approach incorporates crack growth as a function of temperature and applied stress; in other words, the material properties' dependence on temperature.

Conclusions

Several conclusions may be drawn from our work. First, 40-mm-thick LHG8 plates are inherently weaker than 80-mm-thick BK7 plates. This is a non-obvious conclusion because, in general, thicker plates are subjected to higher stresses.

Second, for both LHG8 and BK7, the most adversely stressed areas are the midpoints of the long edges, and there are strong size and rate effects in the buildup of thermal stress during radiative cooling. If all edges have similar crack distributions following finishing, the midpoints of these long edges would then be critical areas of crack growth because they are the most highly stressed.

The third conclusion concerns the choice of the fracture approach. The strength approach is inadequate because strength of a glass surface, let alone of a glass edge, is a parameter that depends on many finishing parameters so that it can hardly be seen as a material property. Even if one could identify a strength value, the case study in the previous section shows that the strength approach would predict that both the LHG8 and BK7 plates would be safe. If anything, the fracture toughness and slow crack growth approaches show that this is not the case.

The fracture toughness approach is a "liberal" criterion, predicting that the worst allowable flaw size in LHG8 would be in the range of 1.9 to 2.7 mm and for BK7 about 2.8 mm.

The slow crack growth criterion is more conservative. It predicts that for LHG8 the worst allowable initial flaw is 0.97 mm deep, while for BK7 it is 1.65 mm.

ACKNOWLEDGMENT

This work was supported by the U.S. Department of Energy Office of Inertial Confinement Fusion under Cooperative Agreement No. DE-FC52-08NA28302, the University of Rochester, and the New York State Energy Research and Development Authority. The support of DOE does not constitute an endorsement by DOE of the views expressed in this article.

REFERENCES

1. W. D. Kingery, J. Am. Ceram. Soc. **38**, 3 (1955).
2. W. D. Kingery, H. K. Bowen, and D. R. Uhlmann, *Introduction to Ceramics*, 2nd ed., Wiley Series on the Science and Technology of Materials (Wiley, New York, 1976), Secs. 16.1–16.3.
3. D. P. H. Hasselman, Ceram. Bull. **49**, 1033 (1970).
4. H. Wang and R. N. Singh, Int. Mater. Rev. **39**, 228 (1994).
5. D. P. H. Hasselman, J. Am. Ceram. Soc. **52**, 600 (2006).
6. J. P. Singh, J. R. Thomas, and D. P. H. Hasselman, J. Am. Ceram. Soc. **63**, 140 (2006).
7. H. Hencke, J. R. Thomas Jr., and D. P. H. Hasselman, J. Am. Ceram. Soc. **67**, 393 (2006).
8. A. G. Tomba-Martinez and A. L. Cavalieri, J. Am. Ceram. Soc. **85**, 921 (2002).
9. A. G. Tomba-Martinez and A. L. Cavalieri, J. Eur. Ceram. Soc. **21**, 1205 (2001).
10. O. Peitel and E. D. Zanotto, J. Non-Cryst. Solids **247**, 39 (1999).
11. J. H. Campbell and T. I. Suratwala, J. Non-Cryst. Solids **263 & 264**, 318 (2000).
12. J. E. DeGroote, A. E. Marino, J. P. Wilson, A. L. Bishop, J. C. Lambropoulos, and S. D. Jacobs, Appl. Opt. **46**, 7927 (2007).
13. T. I. Suratwala *et al.*, J. Non-Cryst. Solids **263 & 264**, 213 (2000).

14. S. M. Wiederhorn and D. E. Roberts, Institute for Materials Research, National Bureau of Standards, Washington, DC, NBS Report 10892, NASA PR 1-168-022, T-5330A (1972).

15. J. C. Lambropoulos, H. Liu, and Y. Wu, "Thermal Shock and Post-Quench Strength of Lapped Borosilicate Optical Glass," to be published in the Journal of Non-Crystalline Solids. See also: Y. Zhang, Y. Wu, H. Liu, and J. C. Lambropoulos, in *Optical Manufacturing and Testing VII*, edited by J. H. Burge, O. W. Faehnle, and R. Williamson (SPIE, Bellingham, WA, 2007), Vol. 6671, p. 66710H.

16. COMSOL® and COMSOL Multiphysics® are registered trademarks of COMSOL AB, Tegnérgatan 23, SE-111 40 Stockholm, Sweden.

17. J. A. Randi, J. C. Lambropoulos, and S. D. Jacobs, Appl. Opt. **44**, 2241 (2005).

18. T. Suratwala *et al*., J. Non-Cryst. Solids **352**, 5601 (2006), see p. 5615, Fig. 15.